CHAPTER 3

Modeling of Doubly Fed Induction Generation (DFIG) Converter Controls

In this chapter, the major effort is devoted to converter controls of DFIG. Differences between drive control and grid integration control are discussed before any presentation of controls. To refresh our memory on drive control, rotor flux-oriented control for an induction machine is first presented, followed by DFIG's rotor-side converter (RSC) control and grid-side converter (GSC) control. With a converter being considered as a controllable AC voltage source with a controllable frequency, magnitude, and phase angle, the entire DFIG system model (with converter controls) can now be built in the *dq*-reference frame.

Modeling and Analysis of Doubly Fed Induction Generator Wind Energy Systems.
http://dx.doi.org/10.1016/B978-0-12-802969-5.00003-2

This chapter presents two simulation examples. The first one is a simulation example in PSCAD with power electronic switching details. The purpose of the demonstration is to show that converter voltage outputs after filters are sinusoidal. Readers can then build visual connections between control of *abc* sinusoidal waveforms versus vector control or control of *dq* variables. The second one is a demonstration of DFIG converter control using the overall DFIG dynamic model.

3.1 ROTOR FLUX-ORIENTED INDUCTION MACHINE CONTROL

Before discussing DFIG converter control, let us review a few concepts related to an induction machine control. Interested readers can refer AC drive textbooks such as [1], for a variety of drive controls, including rotor flux-oriented control and stator flux-oriented control.

From a control engineer's perspective, the first thing to notice is the input/output of the plant: what will be adjusted and which measurements will be used as signals. In the case of induction machine control, we would like to adjust the stator voltage to realize speed control. Therefore, stator voltage is the input of the plant while speed is the output. The stator voltage can be generated by a DC/AC voltage source converter. Through adjusting pulse width modulation (PMW)'s control signals, the output voltage can have a controllable magnitude, frequency, and angle. Note that the output voltage directly from the converter is of discrete voltage levels. It can be decomposed into a fundamental frequency component and higher-order harmonic components with the frequencies at the order of the switching frequency. For an IGBT voltage source converter, the switching frequency is more than ten times of the fundamental frequency. For example, for a 50-Hz system, the switching frequency could be 750 Hz.

Averaging is a modeling and analysis technique popularly applied in power electronics [2]. With switches, converters generate voltages with discrete levels. Through averaging the converter output voltage over a switching period, the higher-order harmonics will all be gone. Only the lower-order harmonics will be considered in modeling. Averaging technique greatly simplifies modeling. It is also reasonable to ignore higher-order harmonics since an inductive filter after the converter or the inductance in windings can get rid of those harmonics. Another benefit of average models is that discrete switching is now ignored from modeling. Average models are continuous dynamic models.

For the analytical models built throughout the textbook, the underlying assumption is that the models are average models. Ultimately, the converter control is expected to generate the stator voltage reference signals. These sinusoidal signals will be fed into the PWM of a VSC to generate pulses to six gates for a typical two-level voltage source converter.

Details of PWM and IGBT switching will not be discussed in this book as these can be found in a typical power electronics textbook. Converters are sensitive to over currents. Therefore, currents through a converter are expected to be regulated very quickly and follow their references. For an induction machine, a constant flux is desired. In summary, an induction machine control should include speed (torque) control, flux control, and current control. In addition, the current control should be much faster than the torque and flux control. Therefore, when designing current control, we can treat the flux and torque as constant, while when we design the torque or flux control, we can assume that the currents can follow their commands immediately. The current control design and the torque/flux control design can be done separately with these assumptions.

3.1.1 Torque/Flux Control

The principal of the decoupled torque/flux control is explained in the following paragraphs. From Chapter 2, we know that the torque can be expressed in terms of air gap flux linkage and the stator current.

$$T_{\mathrm{e}} = \frac{3}{2}\frac{P}{2}\mathcal{R}\left(j\overline{\psi_{\mathrm{m}}}\overline{I_{\mathrm{s}}}^{*}\right) \tag{3.1}$$

Note that the air gap flux linkage and the rotor flux linkage can be related as follows:

$$\overline{\psi_{\mathrm{r}}} = L_{\mathrm{r}}\overline{I_{\mathrm{r}}} + L_{\mathrm{m}}\overline{I_{\mathrm{s}}} \tag{3.2}$$

$$= L_{\mathrm{r}}(\overline{I_{\mathrm{r}}} + \overline{I_{\mathrm{s}}}) - L_{\mathrm{lr}}\overline{I_{\mathrm{s}}} \tag{3.3}$$

$$= \frac{L_{\mathrm{r}}}{L_{\mathrm{m}}}\overline{\psi_{\mathrm{m}}} - L_{\mathrm{lr}}\overline{I_{\mathrm{s}}} \tag{3.4}$$

Therefore, the torque can be expressed in terms of the rotor flux linkage and the stator current.

$$T_{\mathrm{e}} = \frac{3}{2}\frac{P}{2}\mathcal{R}\left(j\frac{L_{\mathrm{m}}}{L_r}\left(\overline{\psi_{\mathrm{r}}} + L_{\mathrm{lr}}\overline{I_{\mathrm{s}}}\right)\overline{I_{\mathrm{s}}}^{*}\right) \tag{3.5}$$

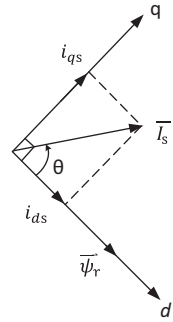

Figure 3.1 Current complex vector decomposed based on the rotor flux-oriented reference frame.

$$= \frac{3}{2}\frac{P}{2}\frac{L_m}{L_r}\mathcal{R}\left(j\overline{\psi_r I_s}^*\right) \tag{3.6}$$

$$= \frac{3}{2}\frac{P}{2}\frac{L_m}{L_r}\left(\psi_{dr} i_{qs} - \psi_{qr} i_{ds}\right) \tag{3.7}$$

It is easily seen in Fig. 3.1 that when the d-axis is aligned with the rotor flux $\overrightarrow{\psi_r}$ ($\overline{\psi_r}$ can be decoupled as $\psi_{dr} = \hat{\psi}_r$ and $\psi_{qr} = 0$), $\overline{I_s}$ can be decoupled as i_{qs} and i_{ds} and the electromagnetic torque T_e is only related to the q-axis stator current i_{qs}.

$$T_e = k\hat{\psi}_r i_{qs} \tag{3.8}$$

where $k = \frac{3}{2}\frac{P}{2}\frac{L_m}{Lr}$. If the rotor flux magnitude $\hat{\psi}_r$ is constant, then T_e and i_{qs} has a linear relationship. If we want to adjust the torque, we can adjust i_{qs} only. On the other hand, we also need to make sure that adjusting i_{qs} will not change the rotor flux magnitude. This can be proved by the following derivation.

The relationship between $\overline{\psi_r}$ and $\overline{I_s}$ is shown below:

$$\overline{\psi_r} = L_r\overline{i_r} + L_m\overline{i_s} \Rightarrow \overline{i_r} = \frac{1}{L_r}(\overline{\psi_r} - L_m\overline{i_s}) \tag{3.9}$$

The relationship between the rotor voltage and the rotor flux is shown as follows:

$$\overline{V_r} = 0 = R_r\overline{i_r} + \frac{d\overline{\psi_r}}{dt} + j\omega_{sl}\overline{\psi_r} \tag{3.10}$$

where ω_{sl} is the slip frequency.

Therefore, for qd-axis variables, we find the following relationship:

$$\begin{cases} 0 = \frac{R_\mathrm{r}}{L_\mathrm{r}}(\psi_{qr} - L_\mathrm{m} i_{qs}) + \frac{\mathrm{d}\psi_{qr}}{\mathrm{d}t} + \omega_{sl}\psi_{dr} \\ 0 = \frac{R_\mathrm{r}}{L_\mathrm{r}}(\psi_{dr} - L_\mathrm{m} i_{ds}) + \frac{\mathrm{d}\psi_{\mathrm{d}r}}{\mathrm{d}t} - \omega_{sl}\psi_{qr} \end{cases} \tag{3.11}$$

Since $\psi_{qr} = 0$, its derivative $\frac{\mathrm{d}\psi_{qr}}{\mathrm{d}t}$ also equals zero. In addition, at steady state, the flux is kept constant. Therefore $\frac{\mathrm{d}\psi_{\mathrm{d}r}}{\mathrm{d}t} = 0$. Thus, we have

$$\omega_{sl} = \frac{R \cdot L_\mathrm{m}}{L_\mathrm{r} \cdot \hat{\psi}_\mathrm{r}} i_{qs} \tag{3.12}$$

$$\psi_{dr} = L_\mathrm{m} i_{ds} \tag{3.13}$$

The rotor flux is related to the d-axis stator current only. Therefore, changing i_{qs} will not impact the steady-state rotor flux magnitude. The aforementioned analysis demonstrates that the torque and flux can be controlled in a decoupled fashion. Given a constant rotor flux, torque is proportional to the q-axis stator current. To track a torque or flux reference, proportional integral controllers are employed to generate the qd-axis current commands. These commands will be tracked by the current controllers.

3.1.2 Inner Current Control

To derive a current control strategy, first of all, we need to find the plant model where the outputs of the plant are current signals and the inputs of the plant model are converter voltages. The control will be based on the rotor flux-oriented reference frame. Therefore, the plant model is also based on the rotor flux-oriented reference frame.

Let us review the relationship between flux linkages and currents.

$$\psi_{qr} = L_\mathrm{r} i_{qr} + L_\mathrm{m} i_{qs} \tag{3.14}$$

$$\psi_{dr} = L_\mathrm{r} i_{dr} + L_\mathrm{m} i_{ds} \tag{3.15}$$

Based on the condition of the rotor flux-oriented reference frame, we know that $\psi_{dr} = \hat{\psi}_r$ and $\psi_{qr} = 0$. Therefore, we have the following relationship between the stator current and the rotor current.

$$i_{qr} = -\frac{L_\mathrm{m}}{L_\mathrm{r}} i_{qs} \tag{3.16}$$

$$i_{dr} = -\frac{L_\mathrm{m}}{L_\mathrm{r}} \left(\hat{\psi}_\mathrm{r} - L_\mathrm{m} i_{ds} \right) \tag{3.17}$$

The stator flux linkages in the rotor flux-oriented reference frame can now be expressed by the stator currents and the rotor flux magnitude solely.

$$\psi_{qs} = \left(L_{\mathrm{s}} - \frac{L_{\mathrm{m}}^2}{L_{\mathrm{r}}}\right) i_{qs} = \sigma L_{\mathrm{s}} i_{qs} \tag{3.18}$$

$$\psi_{ds} = \left(L_{\mathrm{s}} - \frac{L_{\mathrm{m}}^2}{L_{\mathrm{r}}}\right) i_{ds} + \frac{L_{\mathrm{m}}}{L_{\mathrm{r}}}\hat{\psi}_{\mathrm{r}} = \sigma L_{\mathrm{s}} i_{ds} + \frac{L_{\mathrm{m}}}{L_{\mathrm{r}}}\hat{\psi}_{\mathrm{r}} \tag{3.19}$$

where $\sigma = 1 - \frac{L_{\mathrm{m}}^2}{L_{\mathrm{s}} L_{\mathrm{r}}}$.

In the rotor flux-oriented reference frame, the relationship of the stator voltage and the stator current can then be found as follows:

$$v_{qs} = r i_{qs} + \sigma L_{\mathrm{s}} \frac{\mathrm{d}i_{qs}}{\mathrm{d}t} + \sigma \omega L_{\mathrm{s}} i_{ds} + \omega \frac{L_{\mathrm{m}}}{L_{\mathrm{r}}}\hat{\psi}_{\mathrm{r}} \tag{3.20}$$

$$v_{ds} = r i_{ds} + \sigma L_{\mathrm{s}} \frac{\mathrm{d}i_{ds}}{\mathrm{d}t} - \sigma \omega L_{\mathrm{s}} i_{qs} \tag{3.21}$$

where ω is the rotor flux rotating speed. This speed should be the same as the electric frequency in the stator voltage and currents.

Feedforward techniques can be applied to design the current controllers for the *qd*-axis respectively. For simplicity, if we are not keen to have decoupled effect of *qd*-axis current tracking, we can also live with a feedback control without feedforward terms.

Define two variables

$$u_{qs} = v_{qs} - \sigma \omega L_{\mathrm{s}} i_{ds} - \omega \frac{L_{\mathrm{m}}}{L_{\mathrm{r}}}\hat{\psi}_{\mathrm{r}} \tag{3.22}$$

$$u_{ds} = v_{ds} + \sigma \omega L_{\mathrm{s}} i_{qs}. \tag{3.23}$$

Then, we can have two plant models:

$$\frac{i_{qs}}{u_{qs}} = \frac{1}{r + \sigma L_{\mathrm{s}} s} \tag{3.24}$$

$$\frac{i_{ds}}{u_{ds}} = \frac{1}{r + \sigma L_{\mathrm{s}} s} \tag{3.25}$$

We can design the feedback controller in the format of PI control to achieve desired bandwidth. Assume that the PI controller is $K_{\mathrm{P}} + K_i/s$. Then the open-loop transfer function (or loop gain) is

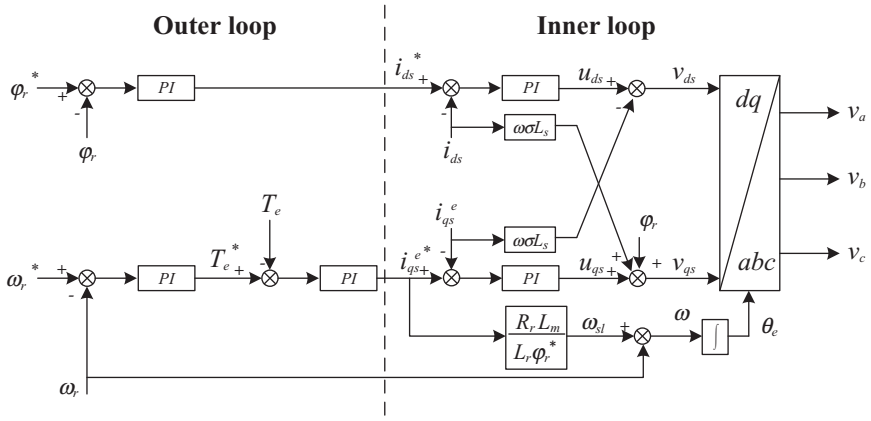

Figure 3.2 Induction machine control block diagram.

$$L(s) = \frac{K_{\mathrm{P}}(s + K_{\mathrm{P}}/K_i)}{s} \frac{1}{r + \sigma L_{\mathrm{s}} s}.$$

Let $K_i/K_{\mathrm{P}} = R/(\sigma L_{\mathrm{s}})$ so that the zero can cancel one of the poles. The loop gain now becomes:

$$L(s) = \frac{K_{\mathrm{P}}}{\sigma L_{\mathrm{s}} s}.$$

The closed-loop transfer function is

$$L_{\mathrm{cl}}(s) = \frac{1}{1 + \frac{\sigma L_{\mathrm{s}}}{K_{\mathrm{p}}} s}$$

If the desired bandwidth is ω_{B}, then $\omega_{\mathrm{B}} = \frac{K_{\mathrm{P}}}{\sigma L_{\mathrm{s}}}$. Based on this relationship, we can determine K_{P} and further determine K_i.

The overall control block diagram shown in Fig. 3.2 includes feedforward terms. The controller parameters can be obtained by trial and error or by analysis.

3.2 DFIG ROTOR SIDE CONVERTER CONTROL

The difference between a grid-integrated DFIG wind turbine and an induction machine resides in control objectives. For a DFIG, the converter

controls are to regulate real power (or torque) and reactive power (or voltage) send to the grid through RSC and GSC's output voltages. RSC's and GSC's AC-side output voltages are the inputs to the plants and the outputs from the converter controls.

DFIG converter controls have been well documented in the literature, *e.g.,* [3]. In this chapter, we will give a brief explanation of the vector control philosophy, the related plant models, and control design.

3.2.1 Outer Control

A RSC is connected to the rotor circuit. Therefore, the rotor currents should also be regulated to avoid overcurrent in the RSC. In that sense, we can reason that the inner current control for a RSC should be the rotor current control, while the outer control should be the real power (torque) and reactive power (ac voltage) control.

Unlike rotor flux-oriented control of an induction machine, DFIG's control relies on stator flux-oriented reference frame ($\psi_{qs} = 0$ or $v_{ds} = 0$). Since DFIG wind turbines are integrated to the grid and the grid voltage can be assumed as constant, the stator flux of the DFIG can be assumed as constant. In the literature, we may find other types of reference frames, e.g., grid flux (flux corresponding to the grid voltage) oriented reference frame, which is also reasonable.

We will express the torque by the stator flux and the rotor current to show that decoupling control is possible for a DFIG. Employing the same technique shown in the previous section, we find that

$$\overline{\psi}_{\mathrm{s}} = L_{\mathrm{s}}\bar{I}_{\mathrm{s}} + L_{\mathrm{m}}\bar{I}_{\mathrm{r}} \tag{3.26}$$

$$= \frac{L_{\mathrm{s}}}{L_{\mathrm{m}}}\overline{\psi}_{\mathrm{m}} - L_{\mathrm{ls}}\bar{I}_{\mathrm{r}} \tag{3.27}$$

Therefore, the torque expression can be found:

$$T_{\mathrm{e}} = \frac{3}{2}\frac{P}{2}\frac{L_{\mathrm{m}}}{L_{\mathrm{s}}}\left(\psi_{qs}i_{dr} - \psi_{ds}i_{qr}\right) \tag{3.28}$$

$$= -\frac{3}{2}\frac{P}{2}\frac{L_{\mathrm{m}}}{L_{\mathrm{s}}}\psi_{ds}i_{qr} \tag{3.29}$$

Note that in this book, we adopt the motor convention. Therefore, when we consider this is a generator, the output power is related to $-T_{\mathrm{e}}$. The

output real power P_s from the stator circuit while ignoring the copper loss can be expressed as

$$P_s = -\omega_e T_e = \frac{3}{2}\frac{P}{2}\omega_e \frac{L_m}{L_s}\psi_{ds} i_{qr} \tag{3.30}$$

where ω_e is the synchronous mechanical speed and $\omega_s = \frac{P}{2}\omega_e$ where ω_s is the electric frequency of the stator.

The reactive power from the stator circuit can be expressed as

$$Q_s = -\frac{3}{2}(v_{qs} i_{ds} - v_{ds} i_{qs}) \approx -\frac{3}{2}\frac{P}{2}\omega_e \psi_{ds} i_{ds} \tag{3.31}$$

Note that $\psi_{ds} = L_m i_{dr} + L_s i_{ds}$. When the stator flux is constant, increase (decrease) in i_{dr} results in increase (decrease) in $-i_{ds}$ or Q_s.

Remarks. The output real and reactive power from the stator circuit can be controlled via i_{qr} and i_{dr} respectively. The outer control can be torque/reactive power or torque/AC voltage. In that case, the generator's torque is also only related to i_{qr}.

3.2.2 Inner Current Control

From the outer power control, rotor current references (of the stator flux reference frame) will be generated. It is through the inner current control that the rotor current commands will be followed by the rotor currents. Feedback control will be employed to realize the command tracking.

We will start from the rotor voltage and rotor flux linkage relationship, then derive the rotor voltage and rotor current relationship, and finally find the plant model for current control.

The complex vector model of the rotor voltage/rotor flux linkage is expressed as follows:

$$\overline{V}_r = r_r \bar{I}_r + \frac{d\overline{\psi}_r}{dt} + j\omega_{sl}\overline{\psi}_r \tag{3.32}$$

$$\begin{cases} v_{qr} = r_r i_{qr} + \frac{d\psi_{qr}}{dt} + \omega_{sl}\psi_{dr} \\ v_{dr} = r_r i_{dr} + \frac{d\psi_{dr}}{dt} - \omega_{sl}\psi_{qr} \end{cases} \tag{3.33}$$

Use the condition of stator flux orientation, we have

$$0 = \psi_{qs} = L_{\mathrm{s}} i_{qs} + L_{\mathrm{m}} i_{qr} \tag{3.34}$$

$$\hat{\psi}_{\mathrm{s}} = \psi_{ds} = L_{\mathrm{s}} i_{ds} + L_{\mathrm{m}} i_{dr}. \tag{3.35}$$

Replace the stator currents in the rotor flux linkage expressions by the rotor currents and stator flux linkages:

$$\psi_{qr} = L_{\mathrm{r}} i_{qr} + L_{\mathrm{m}} i_{qs} = \left(L_{\mathrm{r}} - \frac{L_{\mathrm{m}}^2}{L_{\mathrm{s}}} \right) i_{qr} = \sigma L_{\mathrm{r}} i_{qr} \tag{3.36}$$

$$\psi_{dr} = L_{\mathrm{r}} i_{dr} + L_{\mathrm{m}} i_{ds} = L_{\mathrm{r}} i_{dr} + L_{\mathrm{m}} \frac{\psi_{ds} - L_{\mathrm{m}} i_{dr}}{L_{\mathrm{s}}} = \sigma L_{\mathrm{r}} i_{dr} + \frac{L_{\mathrm{m}}}{L_{\mathrm{s}}} \hat{\psi}_{\mathrm{s}} \tag{3.37}$$

The rotor voltages can now be expressed by the rotor currents only:

$$v_{qr} = r_{\mathrm{r}} i_{qr} + \sigma L_{\mathrm{r}} \frac{\mathrm{d}i_{qr}}{\mathrm{d}t} + \omega_{sl} \left(\sigma L_{\mathrm{r}} i_{dr} + \frac{L_{\mathrm{m}}}{L_{\mathrm{s}}} \hat{\psi}_{\mathrm{s}} \right) \tag{3.38}$$

$$v_{dr} = r_{\mathrm{r}} i_{dr} + \sigma L_{\mathrm{r}} \frac{\mathrm{d}i_{dr}}{\mathrm{d}t} - \omega_{sl} \sigma L_{\mathrm{r}} i_{qr} \tag{3.39}$$

Introduce two virtual variables

$$u_{qr} = v_{qr} - \omega_{sl} \left(\sigma L_{\mathrm{r}} i_{dr} + \frac{L_{\mathrm{m}}}{L_{\mathrm{s}}} \hat{\psi}_{\mathrm{s}} \right) \tag{3.40}$$

$$u_{dr} = v_{dr} + \omega_{sl} \sigma L_{\mathrm{r}} i_{qr} \tag{3.41}$$

The plant models can be found as:

$$i_{qr} = \frac{1}{r_{\mathrm{r}} + \sigma L_{\mathrm{r}} s} u_{qr} \tag{3.42}$$

$$i_{dr} = \frac{1}{r_{\mathrm{r}} + \sigma L_{\mathrm{r}} s} u_{dr} \tag{3.43}$$

Feedback controllers can be designed based on the above two first-order plant models to have desired bandwidths. After the feedback controllers, feedforward compensation should be added back to generate the desired rotor voltages.

The overall control diagram is presented in Fig. 3.3. The inner current control design and the output power control design are carried out in two separate steps with the underlying assumption: the dynamics of the current control is much faster than the power control. Separate control design will be carried out for inner current control and outer power control.

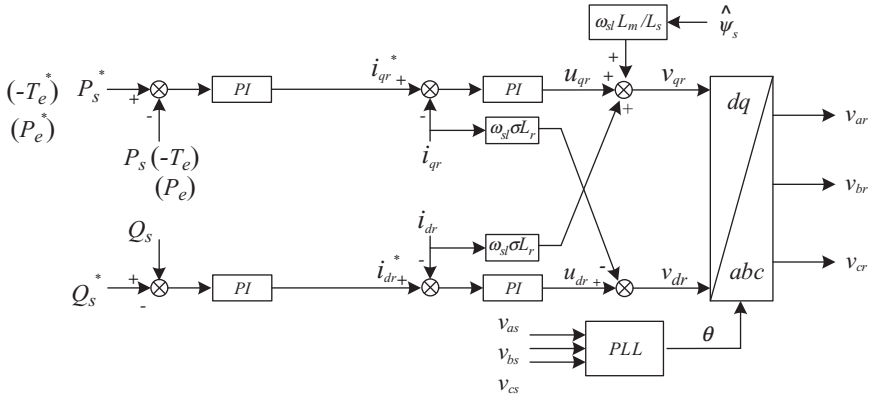

Figure 3.3 DFIG RSC control block diagram.

Indeed, we may be more interested in control of the entire export power or electromagnetic torque from DFIG instead of just the stator power. This can also be done by adjusting i_{qr} only. Recall that

$$P_{\mathrm{s}} = -\omega_{\mathrm{e}} T_{\mathrm{e}} = \frac{3}{2}\frac{P}{2}\omega_{\mathrm{e}}\frac{L_{\mathrm{m}}}{L_{\mathrm{s}}}\psi_{ds} i_{qr}. \tag{3.44}$$

$$P_{\mathrm{e}} = -\omega_{\mathrm{m}} T_{\mathrm{e}} = (1+s)P_{\mathrm{s}} \tag{3.45}$$

If the rotor speed varies much slower than the power control, then we can assume that the slip s is constant and to regulate the entire power P_{e}, we just need to adjust i_{qr}. For a short period of seconds, the wind speed can be assumed as constant. The rotor speed can also be considered as constant.

Additional notes: For the inner current control diagram, the feedforward compensation can be ignored. In that case, to follow a q-axis current command, both qd-axis voltages will be adjusted. Ignoring the feedback compensation makes control simpler and easy to implement. The advantages of feedforward compensation can be found in [4, Chapter 3], including faster start-up transient, decoupling with the AC system, and better disturbance rejection capability.

3.2.3 Maximum Power Point Tracking

Maximum power point tracking (MPPT) can be realized in the RSC control by adjusting the power or torque command. Suppose that the total power

from the DFIG will be controlled. The command of the total power will be generated through the MPPT control block. The input of the control block is the rotor speed ω_m. Through the lookup table, the optimum power corresponding to this speed will be generated. This power will be passed to the outer power control block as the power command.

The ability to get maximum power by the MPPT block is explained as follows. Figure 3.4 presents the wind speed, rotating speed, and mechanical power relationship. The red line (dark grey in print version) is the maximum power curve. Suppose that the wind speed is 9 m/s, the wind generator has a rotating speed lower than the optimum speed. The operating point is notated as Point A, where the optimum operating point is notated as Point B. According to the MPPT lookup table, the generated power command (Point A′) will be less than the current mechanical power. Assuming that the power control dynamics are very fast, the wind turbine now endures a power unbalance: the mechanical power is greater than the electric power. The rotor will speed up until Point B is reached. At Point B, the mechanical power and the electric power command match each other. Similarly, when the wind turbine operates at a rotating speed greater than the optimum speed,

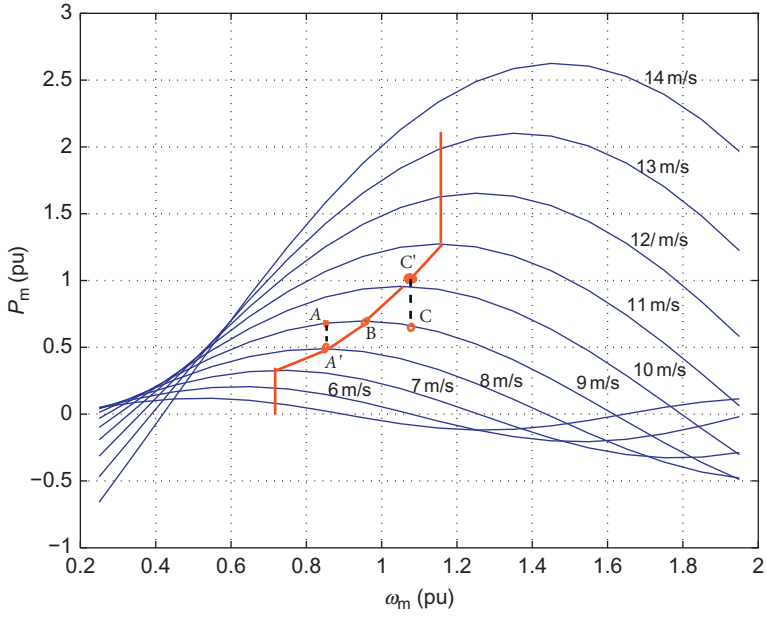

Figure 3.4 MPPT control explanation.

Point C, according to MPPT look up table, the power command should be the same at Point C′. The electric power is now greater than the mechanical power. The rotor should slow down until the operating point reaches B.

3.3 GSC CONTROL

The GSC is connected to the grid through a filter and/or a transformer. The GSC is expected to regulate the AC side voltage/reactive power and to keep the DC-link capacitor voltage constant. With a constant DC-link voltage, the power through the RSC will be the same as that through the GSC. Therefore, this control objective realizes power balance of the converters.

3.3.1 Outer Control

Let the q-axis of the reference frame align with the coupling point voltage $\overrightarrow{e}$ ($e_\mathrm{d} = 0$) and notate the converter output voltage as $\overrightarrow{v}_\mathrm{g}$ or $\overline{V}_\mathrm{g}$. We can then express the real power and reactive power from the GSC to the coupling point as

$$P_\mathrm{g} + jQ_\mathrm{g} = \frac{3}{2}\overline{EI}_\mathrm{g}^{*} \tag{3.46}$$

$$P_\mathrm{g} = \frac{3}{2}(e_q i_{qg} + e_d i_{dg}) = \frac{3}{2} e_q i_{qg} \tag{3.47}$$

$$Q_\mathrm{g} = \frac{3}{2}(e_q i_{dg} - e_d i_{qg}) = \frac{3}{2} e_q i_{dg} \tag{3.48}$$

Therefore, if the coupling point voltage is kept constant (this should be the case for a grid-connected DFIG), real power and reactive power are linearly related to the q-axis and d-axis currents, respectively. We can again design decoupled real power and reactive power control. Keep in mind that the GSC control and RSC control should be coordinated. RSC control has the objective to track the stator active/reactive power commands. Then GSC control should take care of the DC-link voltage.

The DC-link capacitor voltage can be expressed in terms of the power from the RSC and the power leaving the GSC to the grid. The convention of P_r follows the rotor current convention, where injection to the rotor circuit is positive. The convention of P_g follows the GSC current convention, where from the GSC to the grid is positive.

$$\frac{1}{2}C\frac{\mathrm{d}V_\mathrm{dc}^2}{\mathrm{d}t} = -P_\mathrm{r} - P_\mathrm{g} = -\frac{3}{2}\hat{e} i_{qg} - P_\mathrm{r} \tag{3.49}$$

Assuming that the DC-link voltage's variation is small, we have

$$CV_{\mathrm{dc0}}\frac{\mathrm{d}V_{\mathrm{dc}}}{\mathrm{d}t} = -\frac{3}{2}\hat{e}i_{qg} - P_{\mathrm{r}} \tag{3.50}$$

It can be seen that the DC-link voltage can be controlled by adjusting the q-axis current. In this case, positive feedback control should be pursued.

3.3.2 Inner Current Control

The converter is connected to the PCC through an inductor L_{g}. This inductor includes the effect of a filter and/or a transformer. The GSC output voltage, GSC current, and the coupling point voltage have the following relationship expressed in space vector and complex vector.

$$\overrightarrow{v_{\mathrm{g}}} = L\frac{\mathrm{d}\overrightarrow{i}}{\mathrm{d}t} + \overrightarrow{e} \tag{3.51}$$

$$\overline{V}_{\mathrm{g}} = L\frac{\mathrm{d}\bar{I}}{\mathrm{d}t} + \mathrm{j}\omega L_{\mathrm{g}}\bar{I} + \overline{E} \tag{3.52}$$

Align the reference frame's q-axis along with the coupling point voltage $\overrightarrow{e}$, we have

$$v_{qg} = L_{\mathrm{g}}\frac{\mathrm{d}i_{qg}}{\mathrm{d}t} + \omega L_{\mathrm{g}}i_{dg} + e_{\mathrm{q}} \tag{3.53}$$

$$v_{dg} = L_{\mathrm{g}}\frac{\mathrm{d}i_{dg}}{\mathrm{d}t} - \omega L_{\mathrm{g}}i_{qg} \tag{3.54}$$

We can design feedback controllers based on virtual plant inputs $u_{qg} = v_{qg} - \omega L_{\mathrm{g}}i_{dg} - e_{\mathrm{q}}$ and $u_{dg} = v_{dg} + \omega L_{\mathrm{g}}i_{qg}$. The feedback controller has the input from current measurement and generate the desired output u_{qg} and u_{dg}. Through feedforward of cross coupling items, the desired converter voltages can be found.

The overall GSC control is presented in Fig. 3.5. The block LPF stands for a low pass filter which gets rid of high-frequency noise to make the signal smooth. In GSC control, the coupling point voltage is same as the stator voltage.

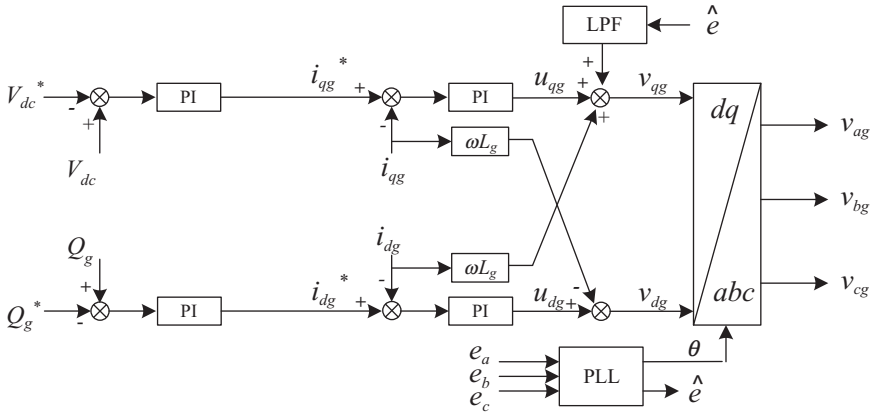

Figure 3.5 DFIG GSC control block diagram.

3.4 COMPLETE DFIG MODELING BLOCKS

RSC and GSC can be considered as two controllable voltage sources. These two voltage sources can be expressed in a reference frame where the stator voltage space vector is aligned with the *q*-axis. Note that the reference frames for DFIG model, RSC control, and GSC control are all aligned with the stator voltage. The RSC and GSC voltages are generated through the afore-mentioned control blocks. In Matlab/Simulink, feedback control blocks can be built. The converter controls can then be integrated with the DFIG model in the same *dq* reference frame.

There is one relationship not modeled yet: the DC-link capacitor dynamics or the relationship between the RSC and the GSC. The DC-link capacitor dynamics has to be considered as well. The overall dynamic model block diagram is shown in Fig. 3.6.

If a DFIG's stator voltage is assumed to be constant, then in the simulation block, v_{qs} can be assumed to be a constant. If the DFIG is connected to an infinity bus through a transmission line which can be considered as series RL components, the transmission line can be regarded as the additional stator resistance and stator leakage inductance. The stator voltage is given from the infinity bus voltage. Should the dynamics of the transmission line are more complicated, then the transmission line has to be adequately modeled. In Chapter 5, dynamics of a transmission line will be modeled and the integrated system model is presented. In Chapter 7, a DFIG

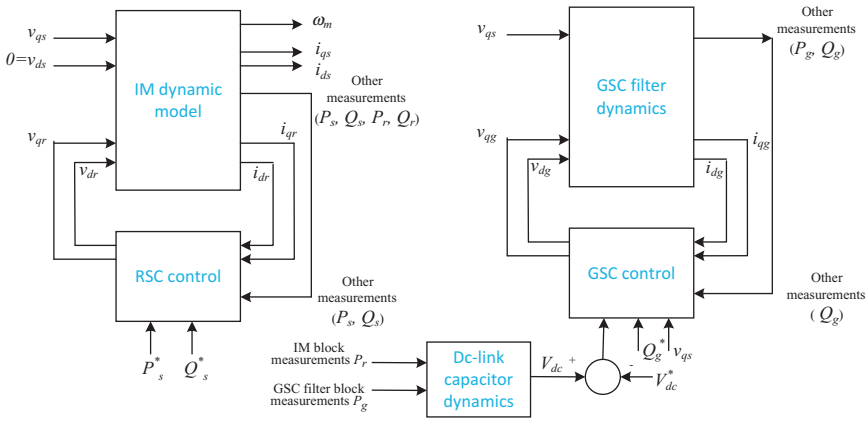

Figure 3.6 Overall DFIG dynamic model block diagram.

is connected to a power grid with multiple synchronous generators. The line dynamics are ignored.

3.5 EXAMPLES

3.5.1 Example 1: PSCAD Simulation of a Two-Level VSC with Sine PWM

In this example, we show PSCAD simulation results of a two-level VSC with sine PWM. The system is shown in Fig. 3.7. The DC side consists of two DC voltage source, each at 100 kV. The DC side is serving an RL three-phase load through a two-level VSC. Six gate signals will be generated through PWM. The phase A voltage (against the ground) v_a, per-phase voltage (E_a, against the neutral point o), and the neutral voltage v_o will be measured.

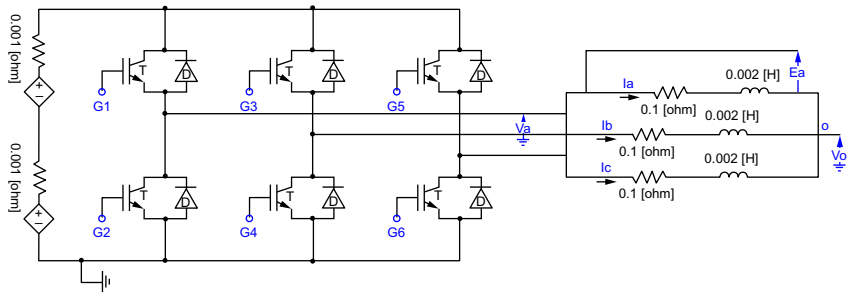

Figure 3.7 A two-level VSC system. DC voltage source: 100 kV.

Figure 3.8 shows the PMW scheme to generate six gate signals. First, three sinusoidal reference signals (magnitude 1, frequency 50 Hz, 120° apart from each other) are generated. The reference signal is then compared with the triangular carrier signal (amplitude 1, frequency 750 Hz). When the reference signal is greater than the carrier signal, the gate signal G1 is 1, G2 is 0. Otherwise, G1 is 0 and G2 is 1. The resulting phase A voltage to the ground is the amplification of the gate signal G1. v_a has two levels: 0 or 200 kV (the DC voltage) as shown in Fig. 3.9. The resulting A to neutral point voltage E_a has five levels as shown in Fig. 3.9. The fundamental component (or the signal after a LPF) is also shown in the first subplot. If we change the frequency and magnitude of the reference signal, we obtain

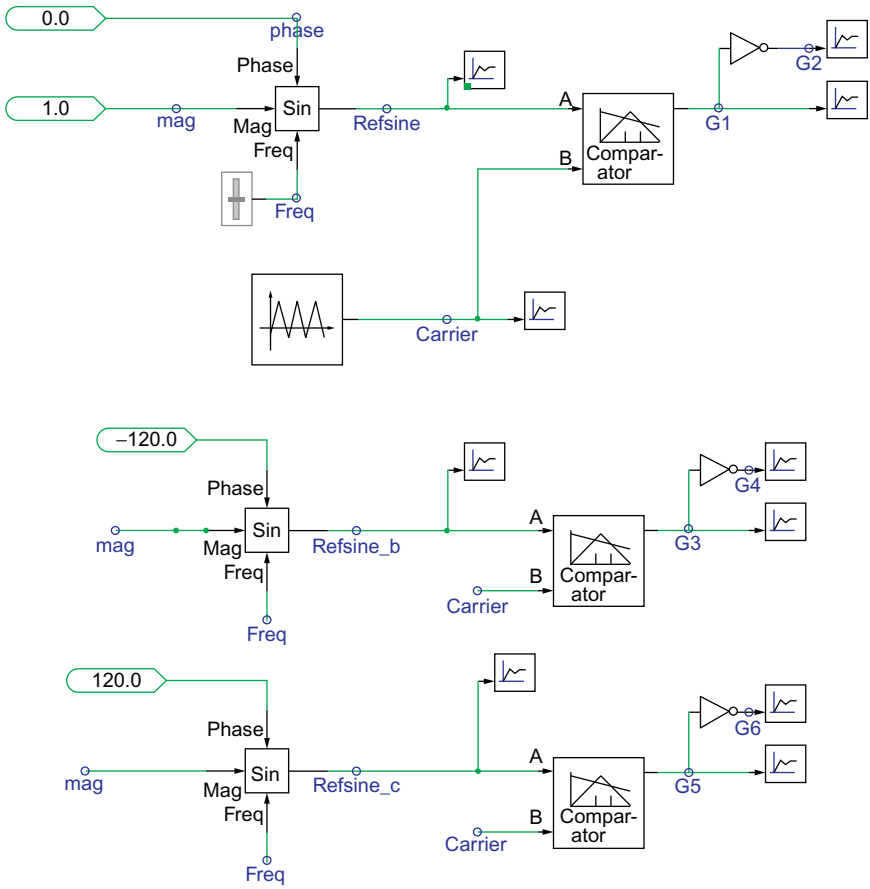

Figure 3.8 Sine PWM schemes for a balanced three-phase output voltage. Modulation index: 1.

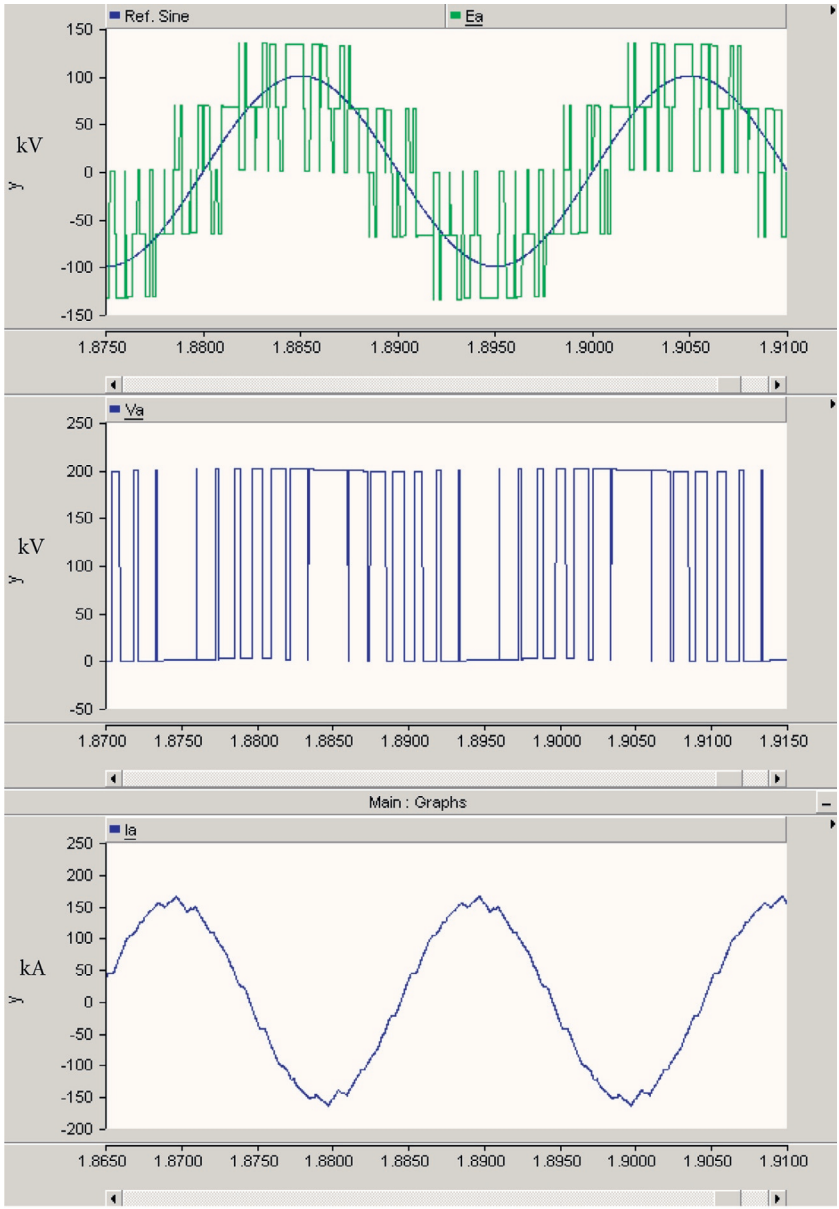

Figure 3.9 Measured signals.

converter voltage with the updated frequency and magnitude. The phase current i_a is shown as almost sinusoidal.

This example gives the PWM switching details and demonstrates that the converter output voltages can be considered as sinusoidal voltages with a fundamental frequency, e.g., 50 Hz. In the mathematical models, the PWM switching details will not be included. Instead, we treat a converter as a controllable three-phase AC voltage source.

3.5.2 Example 2: DFIG Simulation

In the second example, we will use the mathematical model built in Matlab/Simulink to demonstrate DFIG converter control. The dynamic model building follows the diagram shown in Fig. 3.6. The DFIG's parameters are listed in Table 3.1. The slip of the machine is 0.05 pu, which means the DFIG is running below the synchronous speed. Active power will export to the grid through the stator side. However, active power will flow back to the machine rotor ($P_r > 0$, $P_g < 0$) from the grid through GSC and RSC.

Here we assume the stator voltage is constant. At $t = 0.3$ s, the DC-link voltage reference will have a step change. The initial DC voltage reference is 1200 V. After 0.3 s, it becomes 1220 V. We will observe the system dynamic responses in Figs. 3.10–3.12. From Fig. 3.10, it is clear that with GSC control, the DC-link voltage can track the reference. Transients in the DC-link voltage cause transient in the grid converter output active and reactive power.

Table 3.1 Parameters of a Single 2 MW DFIG and the Aggregated DFIG in Network System

Rated power	2 MW
Rated voltage	690 V
X_{ls}	0.09231 pu
X_M	3.95279 pu
X_{lr}	0.09955 pu
R_s	0.00488 pu
R_r'	0.00549 pu
H	3.5 s
X_g	0.3 pu (0.189 mH)
DC-link capacitor C	14,000 μF
DC-link rated voltage	1200 V

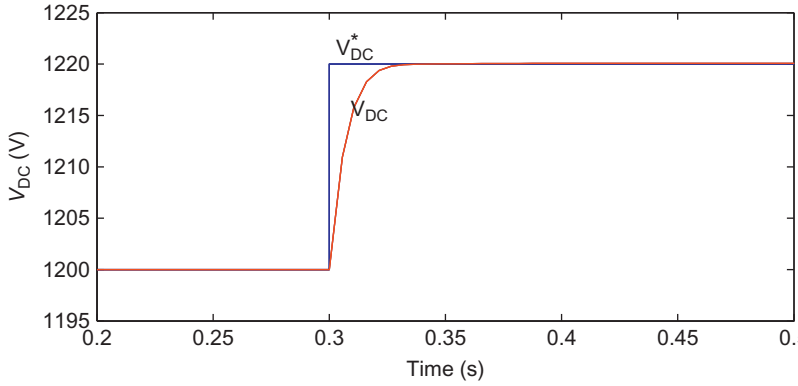

Figure 3.10 DC-Link voltage.

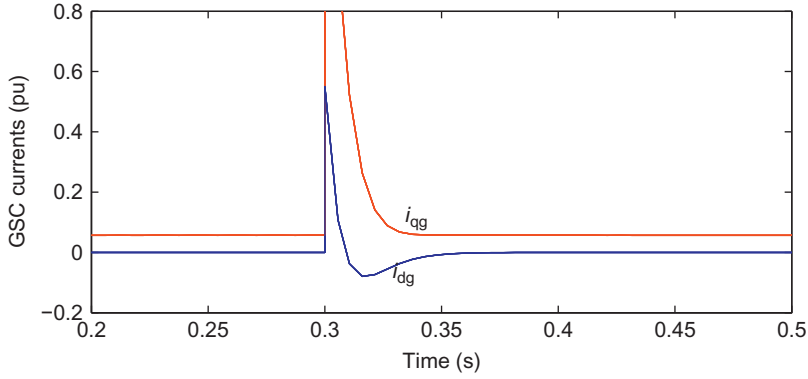

Figure 3.11 GSC qd-axis currents.

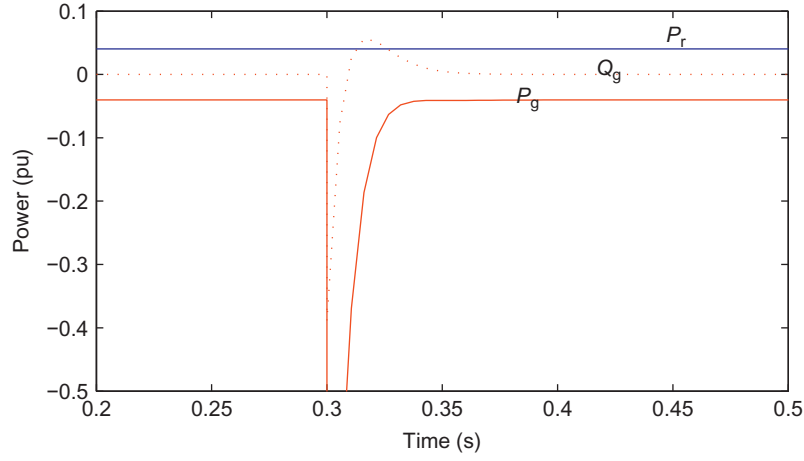

Figure 3.12 Real power from RSC to machine, real and reactive power from GSC to grid.

REFERENCES

[1] B.K. Bose, Modern Power Electronics and AC Drives. Prentice Hall, Upper Saddle River, NJ, 2001.

[2] S.R. Sanders, J.M. Noworolski, X.Z. Liu, G.C. Verghese, Generalized averaging method for power conversion circuits, IEEE Trans. Power Electron. 6(2) (1991) 251-259.

[3] R. Pena, J. Clare, G. Asher, Doubly fed induction generator using back-to-back pwm converters and its application to variable-speed wind-energy generation, IEEE Proc. Electr. Power Appl. 143(3) (1996) 231-241.

[4] A. Yazdani, R. Iravani, Voltage-Sourced Converters in Power Systems: Modeling, Control, and Applications, John Wiley & Sons, New York, 2010.

CHAPTER 4

Analysis of DFIG with Unbalanced Stator Voltage

This chapter presents DFIG analysis during unbalanced stator voltage conditions. The complexity resides in the rotor circuits. In addition, ripples will arise in torque and power. This chapter starts from steady-state circuit analysis, then proceeds to analyze the transient phenomena, and finally presents converter control to mitigate unbalance effect.

4.1 STEADY-STATE HARMONIC ANALYSIS OF A DFIG

The purpose of the analysis is to investigate the DFIG operation at unbalanced stator conditions and study the waveforms of the rotor currents and the electromagnetic torque. It is assumed that sinusoidal voltages are injected into the rotor and that the rotor injection voltage magnitude is constant

Modeling and Analysis of Doubly Fed Induction Generator Wind Energy Systems.
http://dx.doi.org/10.1016/B978-0-12-802969-5.00004-4

during the system disturbance. This assumption simplifies the RSC as a fixed voltage source.

There are two steps in the analysis. The first step is to identify the harmonic components in the rotor currents and the electromagnetic torque. The second step is to estimate the magnitude of each harmonic component.

4.1.1 Steady-State Equivalent Circuit of a DFIG

For analysis, the per-phase steady state equivalent circuit of a DFIG based on [1, 2] is shown in Fig. 4.1. Here N, ω_s and slip are defined based on sequence and harmonic conditions. For example, when $N = 1$, $\omega_s = \omega_e$ and slip $= s$, the circuit corresponds to the well-known positive sequence equivalent circuit of an induction machine.

Remarks.

- positive sequence circuit:

$$\begin{cases} N = 1, \\ \omega_s = \omega_e, \\ \text{slip} = s. \end{cases}$$

- negative sequence circuit:

$$\begin{cases} N = -1, \\ \omega_s = \omega_e, \\ \text{slip} = 2 - s. \end{cases}$$

The derivation of the steady-state circuit for the negative sequence components is given as follows. The equivalent circuit is derived by establishing the relationship of the voltages and currents expressed in *qd*-variables and further in phasors.

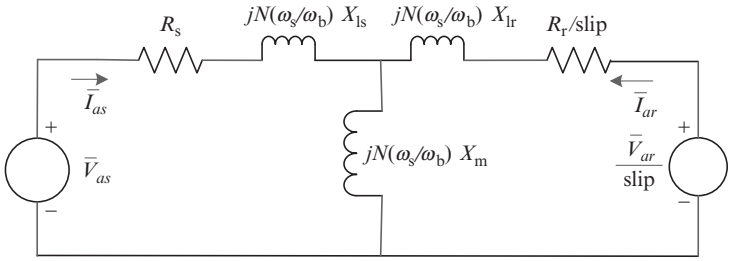

Figure 4.1 Steady-state induction machine circuit representation.

For the negative sequence, the q-axis and d-axis variables become DC variables at steady state when the reference frame rotates at a frequency of $-\omega_e$. The derivatives of the flux linkages are zero at steady state. Hence the voltage and current relationship is expressed in qd as

$$v_{qs}^{-e} = R_s i_{qs}^{-e} - \omega_e \psi_{ds}^{-e} \tag{4.1}$$

$$v_{ds}^{-e} = R_s i_{ds}^{-e} + \omega_e \psi_{qs}^{-e} \tag{4.2}$$

$$v_{qr}^{-e} = R_r i_{qr}^{-e} + (-\omega_e - \omega_m)\psi_{dr}^{-e} \tag{4.3}$$

$$v_{dr}^{-e} = R_r i_{dr}^{-e} - (-\omega_e - \omega_m)\psi_{qr}^{-e} \tag{4.4}$$

The relationship between a phasor $\tilde{F}_{as}$ at a given frequency and the corresponding qd variables in the reference frame rotating at the same frequency can be expressed as:

$$\sqrt{2}\tilde{F}_a = F_q - \mathrm{j}F_d \tag{4.5}$$

where F can be voltages, currents, or flux linkages in the stator or rotor circuits.

Therefore, the stator and rotor voltage, current, and flux linkage relationship can be expressed in phasor form as

$$\tilde{V}_{as}^{-e} = R_s \tilde{I}_{as}^{-e} - j\omega_e \tilde{\psi}_{as}^{-e} \tag{4.6}$$

$$\tilde{V}_{ar}^{-e} = R_r \tilde{I}_{ar}^{-e} - j(\omega_e + \omega_m)\tilde{\psi}_{ar}^{-e} \tag{4.7}$$

The rotor relationship can be further expressed as

$$\frac{\tilde{V}_{ar}^{-e}}{2-s} = \frac{R_r}{2-s}\tilde{I}_{ar}^{-e} - j\omega_e \tilde{\psi}_{ar}^{-e}. \tag{4.8}$$

The equivalent circuit in Fig. 4.1 has $N = -1$, $\omega_s = \omega_e$ and slip $= 2 - s$. If the rotor voltage injection is assumed to be a balanced sinusoidal three-phase set, then the negative component $\tilde{V}_{ar}^{-e} = 0$.

Thus, the stator and rotor currents are induced by both the positive sequence voltages and negative sequence voltages. The rotor currents have two components, one at the low frequency $s\omega_e$ having a root mean square (RMS) magnitude of I_{as+} and the other at the high frequency $(2 - s)\omega_e$ with a magnitude of I_{as-}.

4.1.2 Harmonic Components in Stator and Rotor Currents

The stator frequency is assumed to be 60 Hz. During stator unbalance, the magnitudes of the three phase voltages will not be the same. Also the phase angle displacements of the three voltages will not be 120°. Using symmetric component theory, any three-phase voltages can be decomposed into a positive-, a negative-, and a zero-sequence component. The stator currents will in turn have positive-, negative-, and zero-sequence components.

For an induction machine, the sum of the rotor injection frequency and the rotor rotating frequency equals to the stator frequency or $\omega_r + \omega_m = \omega_s$. For the positive sequence voltage set with frequency ω_s applied to the stator side, the resulting rotor currents have a frequency $\omega_r = \omega_s - \omega_m = s\omega_s$, or slp frequency ω_{sl}.

The negative sequence voltage set can be seen as a three-phase balanced set with a negative frequency $-\omega_s$. Thus the induced flux linkage in rotor circuit and the rotor currents have a frequency of $-\omega_s - \omega_m = -(2 - s)\omega_s$.

Observed from the synchronous reference frame $qd+$ with a rotating speed ω_e, the first component (positive sequence) has a frequency of $s\omega_s - (\omega_e - \omega_m) = 0$, or a DC component, and the second component has a frequency of $-(2 - s)\omega_s - (\omega_e - \omega_m) = -2\omega_e$, i.e., 120 Hz. Observed from the negative synchronous reference frame qd^- which rotates clockwisely with the synchronous speed ω_e, then the positive sequence component has a frequency of $s\omega_s - (-\omega_e - \omega_m) = 2\omega_e$, and the negative sequence component has a frequency of $-(2 - s)\omega_s - (-\omega_e - \omega_m) = 0$. The two reference frames are shown in Fig. 4.2 and Table 4.1 shows the components of the rotor currents in *abc* and the two reference frames.

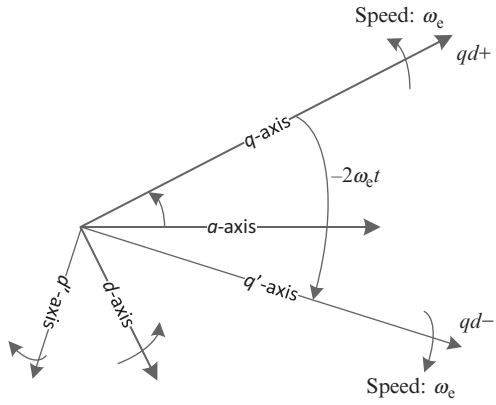

Figure 4.2 The two reference frames: synchronous and negatively synchronous.

Table 4.1 Rotor Current Components Observed in Various Reference Frames

	abc	qd^+	qd^-
Positive	$s\omega_e$	0	$2\omega_e$
Negative	$-(2-s)\omega_e$	$-2\omega_e$	0

The rotor currents in both reference frames will have a DC component and a high frequency component. To extract the harmonic components in the rotor currents, both a synchronous reference frame qd^+ and a clockwise synchronously rotating reference frame qd^- (Fig. 4.2) will be used. A LPF with a suitable cutoff frequency can be used to extract the DC components which correspond to the magnitudes of the two harmonic components. The scheme for extracting the DC components is shown in Fig. 4.3.

4.1.3 Harmonic Components and Magnitudes of Electromagnetic Torque

The zero sequence stator currents will not induce a torque [2]. Meanwhile, the 0-axis stator circuit and 0-axis rotor circuit are completely decoupled. Hence, the 0-axis variable transformed from stator side will not induce any voltage at rotor side. In most machines, wye connection is used so even the stator side will have no zero sequence currents.

Under unbalanced stator condition, the stator current has two components: positive sequence $\bar{I}_{s+}$ and negative sequence components $\bar{I}_{s-}$. The rotor current also has two components: positive sequence $\bar{I}_{r+}$ and negative sequence components $\bar{I}_{r-}$. The electromagnetic torque is produced by the interactions between the stator and rotor currents. The torque can be decomposed into four components:

$$T_e = T_{e1} + T_{e2} + T_{e3} + T_{e4} \tag{4.9}$$

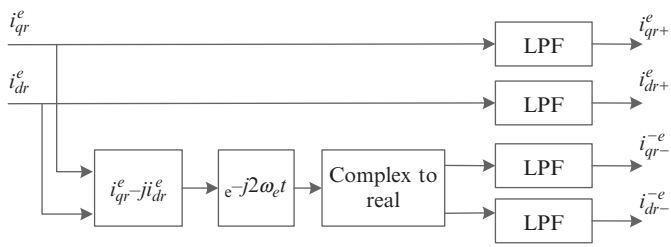

Figure 4.3 Scheme for extracting DC components.

where T_{e1} is due to the interaction of $\bar{I}_{s+}$ and $\bar{I}_{r+}$, T_{e2} is due to the interaction of $\bar{I}_{s-}$ and $\bar{I}_{r-}$, T_{e3} is due to the interaction of $\bar{I}_{s+}$ and $\bar{I}_{r-}$, and T_{e4} is due to the interaction of $\bar{I}_{s-}$ and $\bar{I}_{r+}$.

It will be convenient to use both the synchronously rotating reference frame and the negative synchronous reference frame to compute T_{e}. For example, T_{e1} can be identified as a DC variable. T_{e2} can be identified as a DC variable. T_{e3} and T_{e4} are pulsating torques with a frequency $2\omega_{\mathrm{e}}$. The expressions for the torque components are as follows:

$$T_{e1} = 3\left(\frac{P}{2}\right) X_{\mathrm{m}} \mathcal{I}(\bar{I}^{e}_{s+} \bar{I}^{*e}_{r+}) \tag{4.10}$$

$$T_{e2} = 3\left(\frac{P}{2}\right) X_{\mathrm{m}} \mathcal{I}[\bar{I}^{-e}_{s-} \bar{I}^{*-e}_{r-}] \tag{4.11}$$

$$T_{e3} = 3\left(\frac{P}{2}\right) X_{\mathrm{m}} \mathcal{I}[\bar{I}^{e}_{s+} \bar{I}^{*e}_{r-}] \tag{4.12}$$

$$= 3\left(\frac{P}{2}\right) X_{\mathrm{m}} \mathcal{I}[\bar{I}^{e}_{s+} \bar{I}^{*-e}_{r-} \mathrm{e}^{\mathrm{j}2\omega_{\mathrm{e}}t}] \tag{4.13}$$

$$T_{e4} = 3\left(\frac{P}{2}\right) X_{\mathrm{m}} \mathcal{I}[\bar{I}^{e}_{s-} \bar{I}^{*e}_{r+}] \tag{4.14}$$

$$= 3\left(\frac{P}{2}\right) X_{\mathrm{m}} \mathcal{I}[\bar{I}^{-e}_{s-} \bar{I}^{*e}_{r+} \mathrm{e}^{-\mathrm{j}2\omega_{\mathrm{e}}t}] \tag{4.15}$$

where $\bar{I}_{\mathrm{s}} = 1/\sqrt{2}(i_{qs} - ji_{ds})$ and $\bar{I}_{r} = 1/\sqrt{2}(i_{qr} - ji_{dr})$, and F^{e}_{+} is the qd variables of the positive sequence component in synchronous reference frame; F^{e}_{-} is the qd variables of the negative sequence component in synchronous reference frame; F^{-e}_{+} is the qd variables of the positive sequence component in negative synchronous reference frame; F^{-e}_{-} is the qd variables of the positive sequence component in negative synchronous reference frame.

The torque expression under unbalanced stator condition is

$$T_{\mathrm{e}} = T_{e0} + T_{e\sin 2}.\sin(2\omega_{\mathrm{s}}t) + T_{e\cos 2}.\cos(2\omega_{\mathrm{s}}t) \tag{4.16}$$

where the expression of T_{e0}, $T_{e\sin 2}$ and $T_{e\cos 2}$ can be found in (4.17).

$$\begin{bmatrix} T_{e0} \\ T_{esin2} \\ T_{ecos2} \end{bmatrix} = \frac{3PX_m}{4} \begin{bmatrix} i^e_{qs+} & -i^e_{ds+} & i^{-e}_{qs-} & -i^{-e}_{ds-} \\ i^{-e}_{ds-} & i^{-e}_{qs-} & -i^e_{ds+} & -i^e_{qs+} \\ i^{-e}_{qs-} & -i^{-e}_{ds-} & i^e_{qs+} & -i^e_{ds+} \end{bmatrix} \begin{bmatrix} i^e_{dr+} \\ i^e_{qr+} \\ i^{-e}_{dr-} \\ i^{-e}_{qr-} \end{bmatrix} \quad (4.17)$$

The harmonic components in the torque can be computed from positive and negative stator/ rotor currents.

4.1.4 Example

A 3HP DFIG is used for analysis and simulation. The machine parameters are shown in Table 4.2 as follows.

The initial condition of the machine is the stalling state. A balanced three-phase voltage and a mechanical torque 10 Nm are applied to the stator at $t = 0$ second. The system configuration is shown in Fig. 4.4. At $t = 1$ second, the voltage of phase A drops to zero. The fault is cleared at $t = 1.5$ second. The simulation is performed in Matlab/Simulink and the results are shown in Figs. 4.5–4.7.

Table 4.2 Induction Machine Parameters

$R_s(\Omega)$	0.435
X_{ls} (Ω)	0.754
X_m (Ω)	26.13
X_{lr} (Ω)	0.754
r_r (Ω)	0.816
$J(kg.m^2)$	0.089

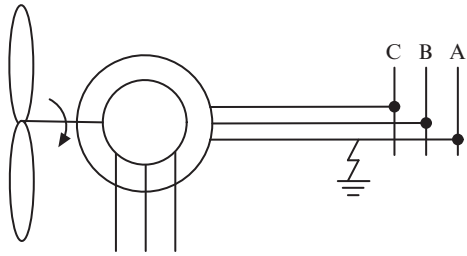

Figure 4.4 A grid-interconnected DFIG system configuration.

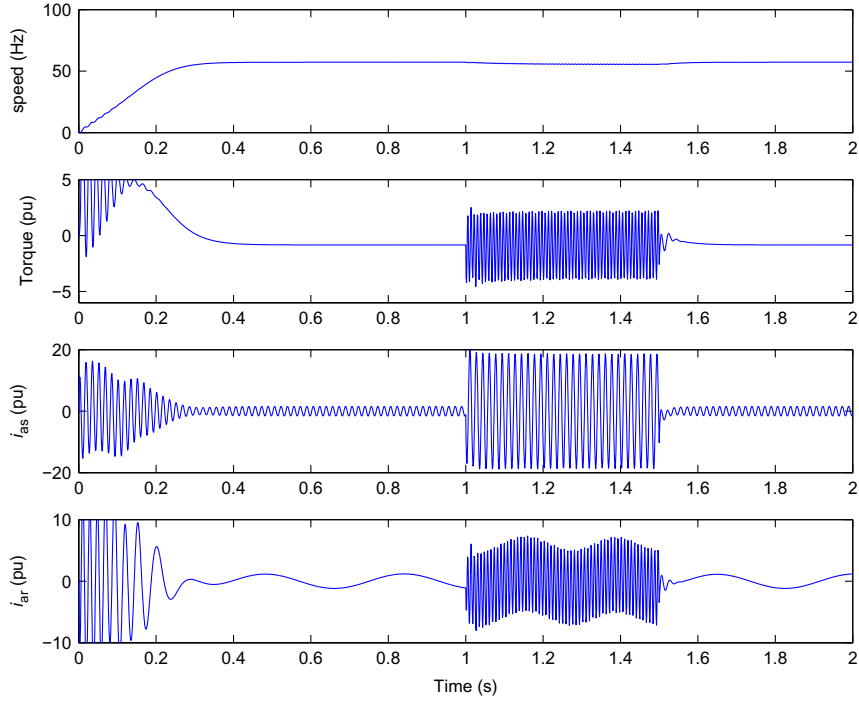

Figure 4.5 Dynamic responses of rotor speed, electromagnetic torque, phase a stator current, and phase a rotor current.

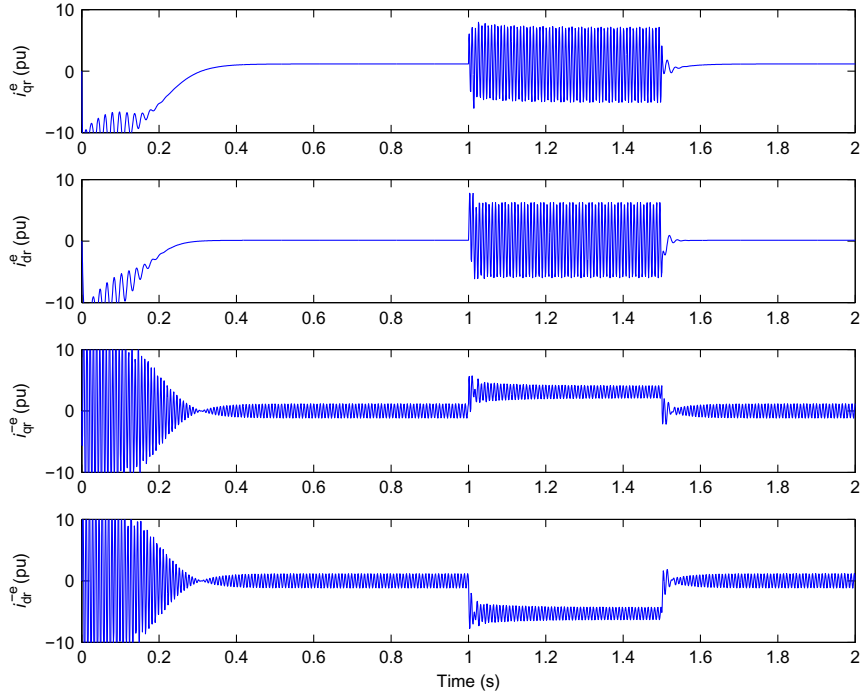

Figure 4.6 Dynamic response of i^{e}_{qr}, i^{e}_{dr}, i^{-e}_{qr}, and i^{-e}_{dr}.

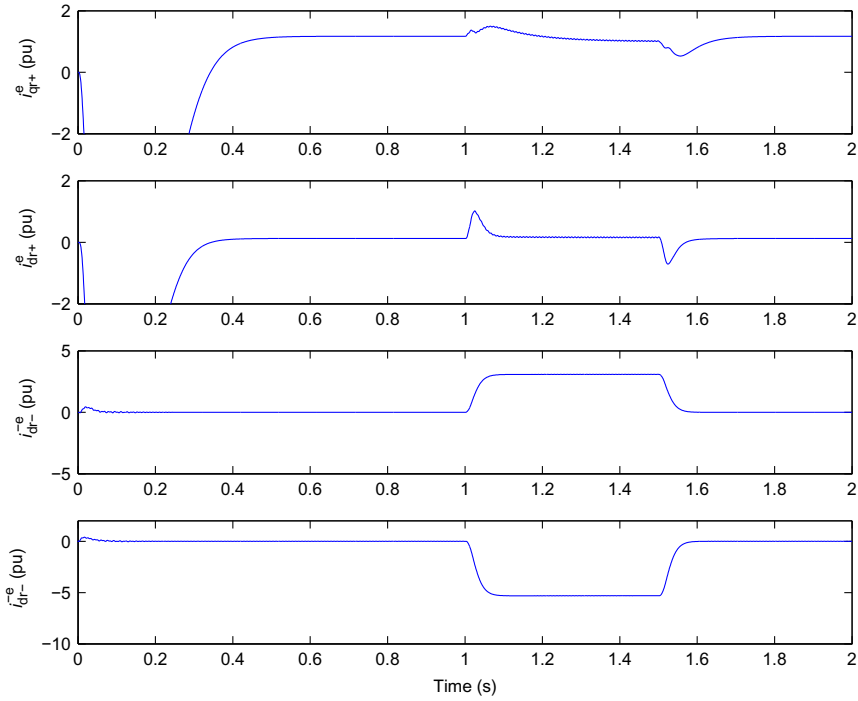

Figure 4.7 Harmonic components after extracting strategy from Fig. 4.3. (a) i^e_{qr+}—DC component of i_{qr} observed in the synchronously rotating reference frame, (b) i^e_{dr+}—DC component of i_{dr} observed in the synchronously rotating reference frame, (c) i^{-e}_{qr-}—DC component of i_{qr} observed in the negatively synchronously rotating reference frame, (d) i^{-e}_{dr-}—DC component of i_{dr} observed in the synchronously rotating reference frame.

Figure 4.5 shows the dynamic responses of the rotor speed, electromagnetic torque, and stator and rotor currents in phase A. Figure 4.6 shows the dynamic responses of the rotor currents in the synchronous reference frame and the negative synchronous reference frame. At the steady state balanced stator condition, the rotor speed is equivalent to 57.2 Hz while the slip frequency of the rotor currents is 2.8 Hz. The two add up to 60 Hz. During unbalance, it is found that the torque has a 120 Hz pulsating component. It is seen from the simulation plots that the rotor current consists of two components: a low frequency component and a high frequency component. According to the analysis the two frequencies are the slip frequency and a frequency close to 120 Hz ($(2 - s)\omega_e$). The rotor currents observed in the synchronous reference frame have a DC component and a 120 Hz component.

Table 4.3 Calculated Sequence Components in Stator Voltages, Stator Currents and Rotor Currents Assuming Slip = 0.12

Voltage	Mag	Current	Mag	Current	Mag	Frequency
$\lvert V_s^+ \rvert$	88.53 V	$\lvert I_s^+ \rvert$	4.78 A	$\lvert I_r^+ \rvert$	4.16 A	$s\omega_e$
$\lvert V_s^- \rvert$	44.26 V	$\lvert I_s^- \rvert$	25.87 A	$\lvert I_r^- \rvert$	25.14 A	$(2-s)\omega_e$
$\lvert V_s^o \rvert$	44.26 V	$\lvert I_s^o \rvert$	50.85 A	$\lvert I_r^o \rvert$	0 A	0

Table 4.4 Harmonic Components in the Rotor Currents and the Electromagnetic Torque from Simulation and Analysis During Unbalanced Condition (Slip = 4.5/60)

	Simulation	Analysis
i_{qr+}^e	6 A	5.8 A
i_{dr+}^e	0.9 A	0.94 A
$\lvert I_{r+} \rvert$	4.29 A	4.16 A
i_{qr-}^{-e}	17.9 A	17.8 A
i_{dr-}^{-e}	-30.8 A	-30.8 A
$\lvert I_{r-} \rvert$	25.2 A	25.15 A
T_{e0}	-10 N m	-9.89 N m
$\sqrt{T_{esin2}^2 + T_{ecos2}^2}$	35 N m	36.3 N m

The magnitudes of the harmonic components can be computed from the equivalent phasor circuits in Fig. 4.1. Table 4.3 lists the calculated positive, negative, and zero sequence components in the stator voltage, stator current, and rotor current.

The sequence components of the stator voltage, the stator currents, and the rotor currents are listed in Table 4.3. A comparison of the analysis results from the circuit in Fig. 4.1 and simulation results shows that the rotor current and torque components from analysis agree with the simulation results in Table 4.4.

4.2 UNBALANCED STATOR VOLTAGE DROP TRANSIENT ANALYSIS

The transients in rotor voltages due to stator voltage dip are analyzed in [3]. In this section, we use an example to explain the effect of unbalanced stator voltage on the rotor circuit transients.

Example. Express the stator flux linkage when the stator voltage has an unsymmetrical voltage drop.

Solution. Recall Chapter 2 (Example 2) of examining rotor voltage due to stator voltage symmetric drop. Here we again use the space vector model to solve this problem.

The key dynamic equation that relates stator voltage and stator flux linkage is the following equation:

$$\overrightarrow{v_s} = R_s \overrightarrow{i_s} + \frac{d\overrightarrow{\psi_s}}{dt} \tag{4.18}$$

$$\text{where } \overrightarrow{\psi_s} = L_m(\overrightarrow{i_s} + \overrightarrow{i_r}) + L_{ls}\overrightarrow{i_s} \tag{4.19}$$

With the assumption of zero rotor current, the stator flux is only related to the stator current.

$$\overrightarrow{\psi_s} \approx L_s \overrightarrow{i_s} \tag{4.20}$$

Therefore, we have

$$\overrightarrow{v_s} \approx \frac{R_s}{L_s}\overrightarrow{\psi_s} + \frac{d\overrightarrow{\psi_s}}{dt}. \tag{4.21}$$

Let us first consider a symmetric stator voltage. Example 2 in Chapter 2 examined a case of stator voltage dropping to zero. Here, we will consider a more general case where the stator voltage initially has a magnitude of V_1 and after the drop a magnitude of V_2. The amplitude of the voltage waveform, which is the same as the magnitude of the space vector, is assumed to be V_2.

At $t = t_0^-$, the space vector of the stator voltage is $\overrightarrow{v}_s(t) = V_1 e^{j\omega_s t}$. At $t = t_0^+$, the space vector of the stator voltage becomes $\overrightarrow{v}_s(t) = V_2 e^{j\omega_s t}$.

For $t < t_0^-$, let us find the steady-state solution of the stator flux linkage $\overrightarrow{\psi_s}(t)$. We know that it should have a format of $\bar{K}e^{j\omega_s t}$, where $\bar{K}$ is a complex vector. Substituting $\overrightarrow{\psi_s}$ by $\bar{K}e^{j\omega_s t}$ in (4.21), we have

$$\bar{K}_s\left(\frac{R_s}{L_s} + j\omega_s\right)e^{j\omega_s t} = V_1 e^{j\omega_s t}$$

$$\bar{K} = \frac{V_1}{\frac{R_s}{L_s} + j\omega_s} \tag{4.22}$$

If we ignore $R_s \approx 0$, then $\bar{K} = \frac{V_1}{j\omega_s}$. Therefore, $\overrightarrow{\psi_s}(t_0^-) = \frac{V_1}{j\omega_s}e^{j\omega_s t_0}$. Since flux linkages cannot change abruptly, therefore, $\overrightarrow{\psi_s}(t_0^+) = \overrightarrow{\psi_s}(t_0^-)$.

Then for $t \geq t_0^+$, let us find the time-domain expression of the flux linkage. The dynamic relationship between the stator voltage and the stator flux linkage is as follows:

$$V_2 e^{j\omega_s t} = \frac{R_s}{L_s}\overrightarrow{\psi}_s + \frac{d\overrightarrow{\psi}_s}{dt} \tag{4.23}$$

The expression of the stator flux linkage consists of a steady-state term (forced flux) and a homogeneous term (natural flux). The forced flux can be found as

$$\overrightarrow{\psi}_{s,F}(t) = \frac{V_2}{\frac{R_s}{L_s} + j\omega_s} e^{j\omega_s(t-t_0)} \approx \frac{V_2}{j\omega_s} e^{j\omega_s(t-t_0)}. \tag{4.24}$$

The nature flux has the form of

$$\overrightarrow{\psi}_{s,N}(t) = Ke^{\frac{-R_s}{L_s}(t-t_0)}, \tag{4.25}$$

where K is a coefficient.

Using the initial condition that $\overrightarrow{\psi}_s(t_0^+) = \frac{V_1}{j\omega_s} e^{j\omega_s t_0}$, we can find $K = \frac{V_1 - V_2}{j\omega_s} e^{j\omega_s t_0}$.

Therefore, for a symmetric stator voltage drop, the time-domain stator flux linkage has an expression as follow:

$$\overrightarrow{\psi}_s(t) \approx \frac{V_2}{j\omega_s} e^{j\omega_s t} + \frac{V_1 - V_2}{j\omega_s} e^{j\omega_s t_0} e^{\frac{-R_s}{L_s}(t-t_0)} \tag{4.26}$$

We now proceed to investigate the stator flux linkage expression for a non-symmetric stator voltage drop. A non-symmetric three-phase voltage can be decomposed into positive-, negative-, and zero-sequence components. Note that the corresponding space vector for the zero-sequence component is zero. Therefore, the space vector for the stator voltage can be expressed in the following:

$$\overrightarrow{v_s}(t) = \begin{cases} V^+ e^{j\omega_s t} + V^- e^{-j\omega_s t}, \text{for } t \geq t_0^+ \\ V_s e^{j\omega_s t}, \text{for } t \leq t_0^- \end{cases} \tag{4.27}$$

The forced flux linkage due to the positive sequence component of the stator voltage is $\frac{V^+}{j\omega_s} e^{j\omega_s t}$. The forced flux linkage due to the negative sequence component is $\frac{V^-}{-j\omega_s} e^{-j\omega_s t}$. And the natural flux linkage is $Ke^{\frac{-R_s}{L_s}(t-t_0)}$.

Using the initial condition, we can find

$$K = \frac{V_s - V^+}{j\omega_s} e^{j\omega_s t_0} + \frac{V^-}{j\omega_s} e^{-j\omega_s t_0}. \tag{4.28}$$

The complete expression of the stator flux linkage is presented as follows:

$$\vec{\psi}_s(t) = \frac{V^+}{j\omega_s} e^{j\omega_s t} + \frac{V^-}{-j\omega_s} e^{-j\omega_s t} + \left(\frac{V_s - V^+}{j\omega_s} e^{j\omega_s t_0} + \frac{V^-}{j\omega_s} e^{-j\omega_s t_0} \right) e^{\frac{-R_s}{L_s}(t-t_0)} \tag{4.29}$$

4.3 CONVERTER CONTROL TO MITIGATE UNBALANCE EFFECT

Transients in rotor voltages due to unsymmetrical stator voltage dip have been analyzed in [3]. Section 4.2 provides a brief analysis on its effect in stator flux. Suitably sized converters can accommodate transients. On the other hand, the more severe operation problems are the torque ripples and the DC-link voltage ripples due to the negative sequence components in the stator and rotor currents [4]. The steady-state analysis of ripples in rotor currents and electromagnetic torque is presented in Section 4.1. In summary, due to unbalanced stator voltage conditions, negative-sequence components in stator currents induce a high frequency component $(\omega_e + \omega_m)$ or $(2-s)\omega_e$ in rotor currents and pulsations at $2\omega_e$ frequency in electromagnetic torques. In this section, negative sequence compensation techniques via RSC and GSC are presented.

4.3.1 Negative Sequence Compensation via GSC

Negative sequence compensation via GSC is presented in [5]. The philosophy is to let the GSCs compensate the negative sequence currents required in the network during any unbalanced operation. The circuit model is shown in Fig. 4.8. The GSCs will supply the negative sequence current components to the grid. Hence the stator currents will remain balanced. With balanced stator currents, a rotating magnetic field will be formed in the air gap, which induces balanced EMF in the rotor circuits. The rotor currents will remain balanced. Therefore, the torque will remain ripple free.

For negative sequence compensation via GSC, the current controllers of the GSC will measure the network currents, extract the negative sequence components and generate the required negative sequence currents from the GSC for compensation. The reference values of the negative sequence

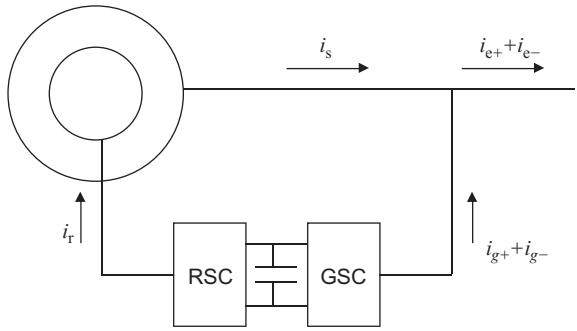

Figure 4.8 The control philosophy: negative sequence compensation through GSC: $i_{g-} = i_{e-}$. Stator current i_s is free of negative sequence components.

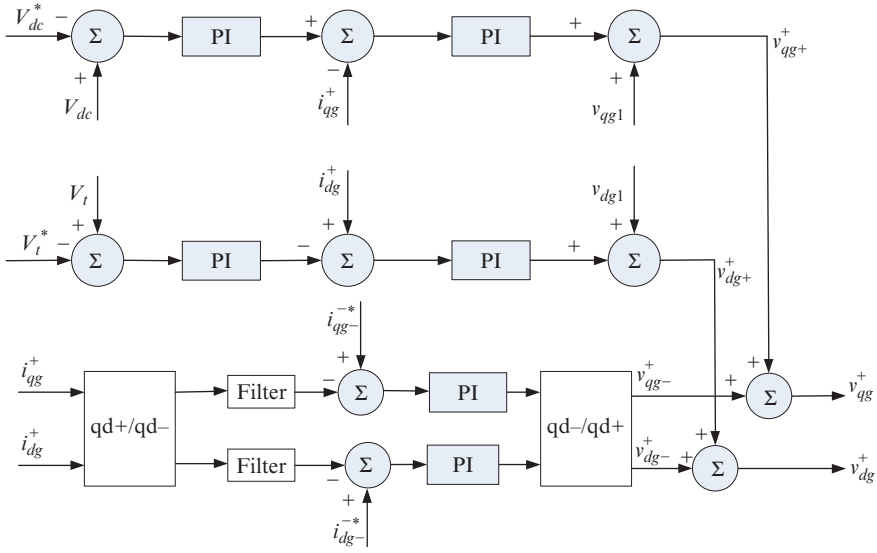

Figure 4.9 Dual sequence control loops of GSC. $v_{qg1} = v_{qs} + \omega_e L_g i_{dg}$; $v_{dg1} = v_{ds} - \omega_e L_g i_{dg}$. L_g is the inductance of the transformer connecting the GSC to the grid.

currents come from the measurements of the currents to the grid $i_{e,abc}$. The negative sequence components of $i_{e,abc}$ are then extracted through abc/qd^- transformation and LPFs.

Figure 4.9 presents the dual sequence control loops of GSC. The positive-sequence control loop is the same as the control loop presented in Chapter 3. In addition, the negative-sequence control loop generates negative-sequence voltage. The assumption of Fig. 4.9 is that all measurements are available

in the synchronous reference frame $dq+$. For the negative-sequence control, the currents are first been transformed in the dq-reference frame. In that reference frame, the negative-sequence current component appears as DC variables while the positive-sequence component appears as 120 Hz ripple. With a LPF, only the negative-sequence current component (i_{qg}^{-}, i_{dg}^{-}) will be obtained. For the given reference values, PI controllers are suitable to the measurements to track the reference values. The output from the PI controllers are negative-sequence voltage in $dq-$ frame. This component should be transformed back to $dq+$ and added back to the voltage generated by the positive-sequence control.

4.3.1.1 Drawbacks of GSC Compensation

Since the GSC compensates a negative sequence current to the grid, the three-phase voltage from the GSC should provide the negative sequence component as well. The instantaneous power through the GSC will have pulsating components. The dynamic equation of DC-ink voltage is given by:

$$CV_{\mathrm{DC}}\frac{\mathrm{d}V_{\mathrm{DC}}}{\mathrm{d}t} = -P_{\mathrm{g}} - P_{\mathrm{r}} \tag{4.30}$$

where P_{g} and P_{r} are the GSC and RSC instantaneous powers. The directions of the powers are determined by the direction of the currents in Fig. 4.8.

The detailed analysis of the DC-link voltage due to unbalanced grid voltages can be found in [6]. If there is only negative sequence compensation from the GSC, and with the assumption that the rotor power P_{r} has only DC component, the DC-link voltage will have ripples with two pulsating components at frequencies of $2\omega_{\mathrm{e}}$ and $4\omega_{\mathrm{e}}$ [6]. The more unbalanced the grid voltage, the higher the magnitude of the pulsating power, and hence the higher the magnitude of the DC-link voltage ripple.

4.3.2 Negative Sequence Compensation via RSC

Torque pulsation can be eliminated by negative sequence compensation via the RSC [7, 8]. The steady-state negative sequence circuit model with the RSC compensation has been derived in Section 4.1 (Fig. 4.1). From the circuit model, it can be seen that for a given negative-sequence stator voltage, a negative sequence rotor voltage generated the RSC has the potential to eliminate the negative sequence rotor current ($\bar{I}_{ar}^{-} = 0$) or the negative sequence stator current ($\bar{I}_{as}^{-} = 0$) or the torque pulsation. The derivation of the rotor current reference values to eliminate the torque

pulsation can be found in [7]. In the following paragraphs, torque pulsation elimination procedure will be described.

The control objective is to eliminate the ripples in the torque and therefore the reference values of the negative sequence rotor currents need to be calculated. The electromagnetic torque can be expressed in the form of the stator flux linkage and the rotor current [2]:

$$T_{\mathrm{e}} = \frac{3}{2}\frac{P}{2}\frac{L_{\mathrm{m}}}{L_{\mathrm{s}}}\Re(-j\overrightarrow{\psi_{\mathrm{s}}}\,\overrightarrow{i_r^*}) \tag{4.31}$$

The rotor current space vector and the stator flux linkage space vector in qd^+ reference frame consisting of positive and negative sequence components can be expressed as follows:

$$\begin{cases} \overrightarrow{I_{\mathrm{r}}}^{+} = \overline{I_{\mathrm{r}}}_{+}^{+} + \overline{I_{\mathrm{r}}}_{-}^{-}\mathrm{e}^{-\mathrm{j}2\omega_{\mathrm{e}}t} \\ \overrightarrow{\psi_{\mathrm{s}}}^{+} = \overline{\psi_{\mathrm{s}}}_{+}^{+} + \overline{\psi_{\mathrm{s}}}_{-}^{-}\mathrm{e}^{-\mathrm{j}2\omega_{\mathrm{e}}t}. \end{cases} \tag{4.32}$$

Therefore, the electromagnetic torque in (4.31) has three components: $T_{\mathrm{e}}^{+} = T_{e\mathrm{dc}}^{+} + T_{e\cos}^{+}\cos(2\omega_{\mathrm{e}}t) + T_{e\sin}^{+}\sin(2\omega_{\mathrm{e}}t)$,

$$\text{where} \begin{cases} T_{e\mathrm{dc}}^{+} = K(\psi_{qs+}^{+}i_{qr+}^{+} + \psi_{ds+}^{+}i_{dr+}^{+} + \psi_{qs-}^{-}i_{qr-}^{-} + \psi_{ds-}^{-}i_{dr-}^{-}) \\ T_{e\cos}^{+} = K(\psi_{qs+}^{+}i_{qr-}^{-} + \psi_{ds+}^{+}i_{dr-}^{-} + \psi_{qs-}^{-}i_{qr+}^{+} + \psi_{ds-}^{-}i_{dr+}^{+}) \\ T_{e\sin}^{+} = K(\psi_{ds+}^{+}i_{qr-}^{-} - \psi_{qs+}^{+}i_{dr-}^{-} - \psi_{ds-}^{-}i_{qr+}^{+} + \psi_{qs-}^{-}i_{dr+}^{+}) \end{cases} \tag{4.33}$$

where $K = \frac{3}{2}\frac{P}{2}\frac{M}{L_{\mathrm{s}}}$. To minimize ripples in the electromagnetic torque, the AC components of the torque should be set to zeros, that is,

$$\begin{cases} T_{e\cos}^{+} = 0 \\ T_{e\sin}^{+} = 0. \end{cases} \tag{4.34}$$

From the above requirements, the reference values of the negative sequence rotor currents can be computed based on the reference positive sequence rotor currents and the stator flux linkage measurements. The PI controllers in the negative sequence control loops make sure the negative sequence components in the rotor currents track the referenced values.

Computation of the reference negative sequence currents requires extensive information of the stator flux linkage and the positive sequence

reference rotor current. Time delay will be introduced in such control structure.

4.3.2.1 Dual-Sequence RSC Control

Dual sequence controllers to separately control the positive sequence and negative sequence rotor current applied in [4, 9] are shown in Fig. 4.10. Low pass filters are applied to separate the currents after abc/dq transformation. Filters can introduce time delay and deteriorate control performance. Therefore, in [10, 11], the main controller dealing with the positive sequence is implemented without filter, only the auxiliary controller dealing with the negative sequence rotor currents has filters. Note the negative-sequence rotor current commands are computed from (4.34).

4.3.2.2 Proportional Resonant RSC Control

Instead of realizing dual-sequence control in $dq+$ and $dq-$ reference frame, the control can be realized in one reference frame $\alpha\beta$ reference frame. In the $\alpha\beta$ reference frame, we deal with AC signals. Ac signal tracking can be realized by proportional resonant (PR) control. A PR controller can be considered as an AC signal tracker just as a PI controller is a DC signal tracker [12]. For example, a compensator with a transfer function $K_\mathrm{p}+\frac{K_R s}{s^2+\omega_\mathrm{e}^2}$ can make sure the open-loop function has an infinitive magnitude at ω_e.

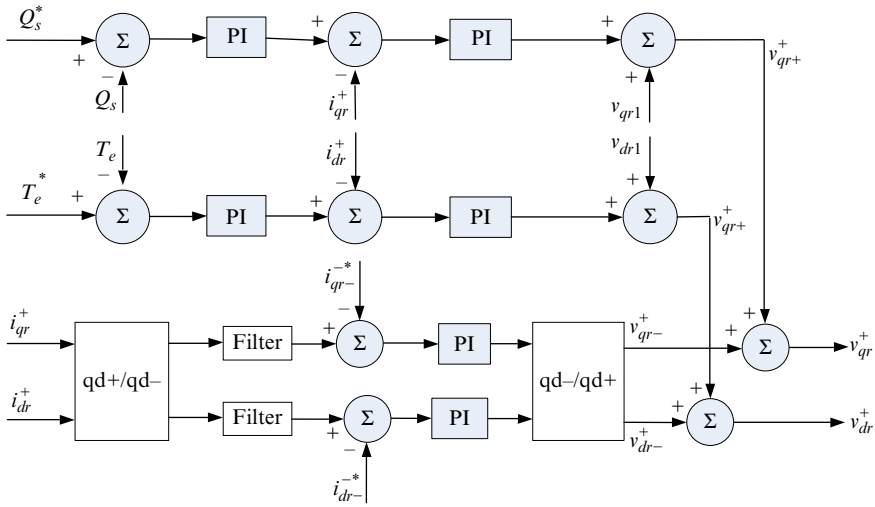

Figure 4.10 Dual sequence control loops for RSC. $v_{qr1} = s\omega_\mathrm{e}\sigma L_\mathrm{r} i_{dr} + s\omega_\mathrm{e}\frac{L_\mathrm{m}}{L_\mathrm{s}}\psi_{ds}$, $v_{dr1} = -s\omega_\mathrm{e}\sigma L_\mathrm{r} i_{qr}$, *where* $\sigma = 1 - \frac{L_\mathrm{m}^2}{L_\mathrm{s}L_\mathrm{r}}$.

Therefore, the close-loop system will realize zero error at that frequency. For a signal with a frequency of ω_e, that PR controller can make the signal track its reference.

In addition, instead of computing the reference values of the RSC negative sequence currents, the reference values for the negative sequence rotor currents can be set to zeros. This way, pulsations in both the rotor currents and the torque can be suppressed if not fully eliminated. Hence, the purpose of the negative sequence RSC current controller is to eliminate the negative sequence rotor currents and the reference negative sequence rotor currents are zero.

With such knowledge, the dual sequence control structure can be simplified using proportional resonance (PR) or proportional integral resonant (PIR) controller. A PR controller has been tested to eliminate the negative sequence rotor current by the authors in [13]. The PR-based control loops for the RSC is shown in Fig. 4.11.

Since the negative sequence current reference values are set to zeros, the reference currents in $\alpha\beta$ contain only positive sequence information. The measurements will also be transferred to $\alpha\beta$ frame. Rotor currents in $\alpha\beta$ will only have components with a frequency of ω_e under unbalanced grid voltage conditions. PR controllers are effective for AC signal tracking. Hence the controller will eliminate the negative sequence currents in the rotor circuits.

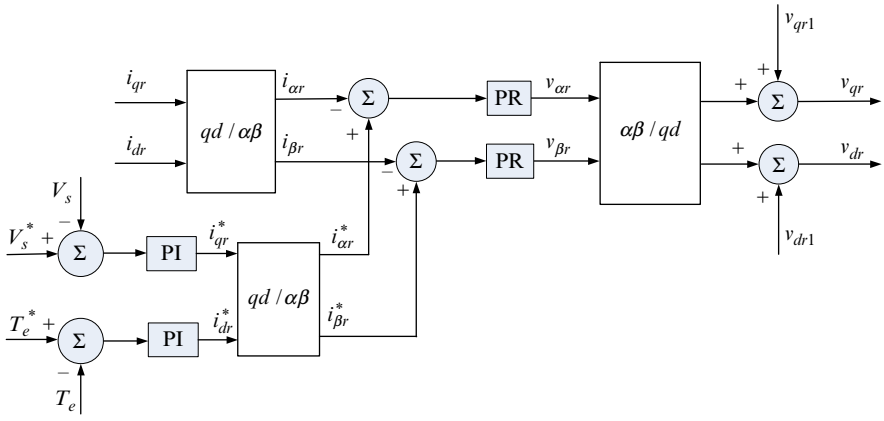

Figure 4.11 Proposed control loops for RSC. The transfer function in the PR block is $K_P + \frac{K_I s}{s^2+\omega_e^2}$. $v_{qr1} = s\omega_e \sigma L_r i_{dr} + s\omega_e \frac{L_m}{L_s}\psi_{ds}$, $v_{dr1} = -s\omega_e \sigma L_r i_{qr}$.

4.3.2.3 Drawbacks of RSC Compensation

Without losing the generality, the RSC needs to inject a negative sequence voltage. Similar as the consequence of negative sequence compensation via GSC, the DC-link voltage will have ripples with pulsating components. Therefore using RSC negative sequence compensation alone leads to DC-link voltage ripples.

It seems that torque ripple suppression and DC-link voltage ripple suppression, cannot be achieved simultaneously using either RSC compensation or GSC compensation. Therefore both RSC and GSC controls are used in [4, 9–11]. Interested readers can consult these references for more information on RSC and GSC coordination under unbalanced conditions.

REFERENCES

[1] A. Fitzgerald, C. Kingsley, A. Kusko, Electric Machinery, McGraw-Hill Book Company, New York, 1971.

[2] P. Krause, Analysis of Electric Machinery, McGraw-Hill, New York, 1986.

[3] J. Lopez, E. Gubia, P. Sanchis, X. Roboam, L. Marroyo, Wind turbines based on doubly fed induction generator under asymmetrical voltage dips, IEEE Trans. Energy Convers. 23(1) (2008) 321-330.

[4] Y. Zhou, P. Bauer, J. Ferreira, J. Pierik, Operation of grid-connected DFIG under unbalanced grid voltage condition, IEEE Trans. Energy Convers. 24(1) (2009) 240-246.

[5] R. Pena, R. Cardenas, E. Escobar, Control system for unbalanced operation of stand-alone doubly fed induction generators, IEEE Trans. Energy Convers. 22(2) (2007) 544-545.

[6] X. Wu, S. Panda, J. Xu, Analysis of the instantaneous power flow for three-phase pwm boost rectifier under unbalanced supply voltage conditions, IEEE Trans. Ind. Electron. 23(4) (2008) 1679-1691.

[7] L. Xu, Y. Wang, Dynamic modeling and control of DFIG-based wind turbines under unbalanced network conditions, IEEE Trans. Power Syst. 22(1) (2007) 314-323.

[8] J. Hu, Y. He, Modeling and enhanced control of DFIG under unbalanced grid voltage conditions, Electric Power Syst. Res. 79(2) (2008) 273-281.

[9] O. Gomis-Bellmunt, A. Junyent-Ferre, A. Sumper, J. Bergas-Jane, Ride-through control of a doubly fed induction generator under unbalanced voltage sags, IEEE Trans. Energy Convers. 23(4) (2008) 1036-1045.

[10] L. Xu, Coordinated control of DFIG's rotor and grid side converters during network unbalance, IEEE Trans. Power Electron. 23(3) (2008) 1041-1049.

[11] L. Xu, Enhanced control and operation of DFIG-based wind farms during network unbalance, IEEE Trans. Energy Convers. 23(4) (2008) 1073-1081.

[12] R. Teodorescu, F. Blaabjerg, M. Liserre, P. Loh, Proportional-resonant controllers and filters for grid-connected voltage-source converters, IEEE Proc. Electr. Power Appl. 153(5) (2006) 750-762.

[13] L. Fan, R. Kavasseri, H. Yin, C. Zhu, M. Hu, Control of DFIG for rotor current harmonics elimination, in: Proceedings of IEEE Power & Energy Society General Meeting, Calgary, Canada, Jul. 2009.